PHOENICS News

CHAM

## PHOENICS – Empowering Engineers

Autumn 2017

This Edition

Articles from PHOENICS Users in this Newsletter describe the "Modelling of Waves Formed from Landslides into the Sea" (pg 6); "Development of a Sustainable System of Decentralized Mechanical Ventilation for Façades" (pg 8) and "Aerosol Deposition Modelling with PHOENICS-FLAIR" (pg 9).

Learn about the "Development of Interface Simulation Methods in PHOENICS" (pg 2) and the development of PHOENICS Marine planned for release early in 2018 (to be beta-tested late 2017) (pg 12).

Read about the "Implementation of Numerical Wave Generation in PHOENICS Marine" (pg 11).
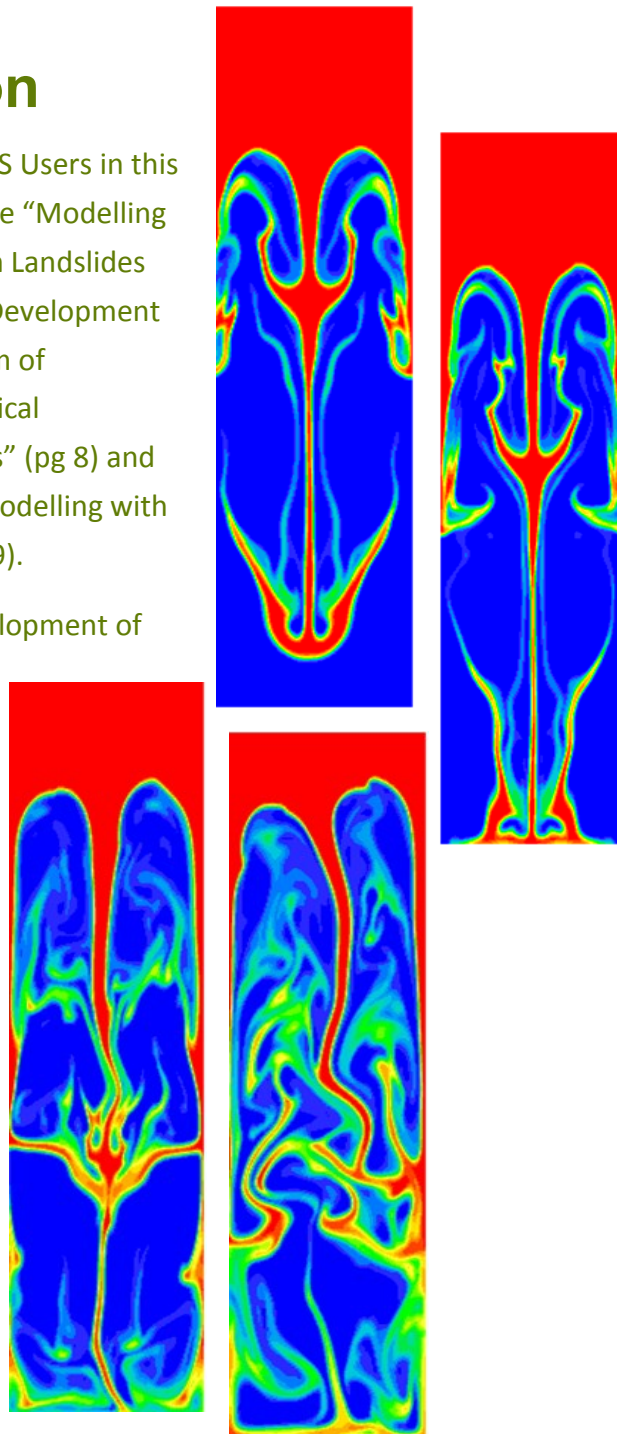
PHOENICS Volume of Fluid (VOF) Method Applied to the Rayleigh Taylor Problem (See pages 4 and 5)

"*The use of PHOENICS and PHOENICS-Flair was central to our work as researchers and was a powerful and advanced tool in this regard. We would like to thank the CHAM Company and especially Mr. Peter Spalding, without which this stage of our research would not have been possible.*"

Marco Aurélio de Oliveira, Director, Confortus Engenharia Acustica (see page 6)

Development of Interface Simulation Methods in PHOENICS

Jalil Ouazzani: Arcofluid Consulting LLC (Orlando, Fl), Arcofluid Sarl, (France)
John C Ludwig: CHAM, London

Introduction

PHOENICS 2018 provides a significant upgrade to its existing Volume-Of-Fluid (VOF) capability which improves considerably the accuracy of the interface resolution for immiscible-fluid and free-surface flows. The upgrade also includes the effects of surface tension at the interface of the two fluids, which are important at low Capillary and Weber numbers. These effects are modelled by using the continuum-surface-force (CSF) model proposed by Brackbill et al (1992).

The VOF method tracks the free surface or fluid-fluid interface by solving a volume-fraction equation on a fixed Eulerian mesh together with a single set of momentum equations shared by the two fluids. The volume fraction equation serves as an indicator to distinguish between these two fluids, but special treatment of the convection terms is required to address the problem of numerical smearing of the interface over several mesh cells, whilst ensuring boundedness of computed volume fractions. Different techniques have been proposed to maintain a well-defined interface, and these can be classified as either geometric-interface-reconstruction methods, donor-acceptor schemes or higher-order discretization schemes.

The latter technique is used in PHOENICS 2018, and the following high-resolution methods have been implemented as options: CICSAM (Compressive Interface Capturing Scheme for Arbitrary Meshes), HRIC (High Resolution Interface Capturing scheme), modified HRIC and STACS (Switching Technique for Advection and Capturing of Surfaces). All of these schemes offer superior interface capturing to the existing Scalar-Equation-Method (SEM).

The most popular high-resolution scheme is CICSAM, proposed by Ubbink et al. (1997 & 1999) for free-surface simulations on unstructured meshes. Later, other schemes based on the same ideas have been derived, such as HRIC (Muzaferija & al. 1998), Modified HRIC (Park & al 2009) and STACS (Darwich & al 2006). Wacławczyk et al (2008) provides a detailed description of the CICSAM and HRIC schemes, as well as their comparison on specific test cases.

The NVD (Normalised Variable Diagram) of Leonard (1991) provides the foundation for the high order schemes CICSAM, HRIC, modified HRIC and STACS. Based on the notation introduced in Figure 1, and the Convective Boundedness Criterion (CBC) $\varphi_D \leq \varphi_f \leq \varphi_A$ for a variable φ on the cell face f, normalized variables are introduced.

$$\widetilde{\phi}_f = \frac{\phi_f - \phi_U}{\phi_A - \phi_U}, \quad \widetilde{\phi}_D = \frac{\phi_D - \phi_U}{\phi_A - \phi_U} \qquad (1)$$

From here it follows that if φ_f is a function of φ_D, φ_A and φ_U, then the normalized variable $\widetilde{\phi}_f$ is only a function of $\widetilde{\phi}_D$ (since $\widetilde{\phi}_A = 1$ and $\widetilde{\phi}_U = 0$. This is the basis of the NVD, which is a plot of the functional relationship between the normalized convected face value $\widetilde{\phi}_f$ and the normalized adjacent donor node value $\widetilde{\phi}_D$.
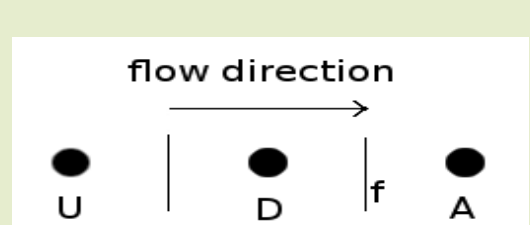

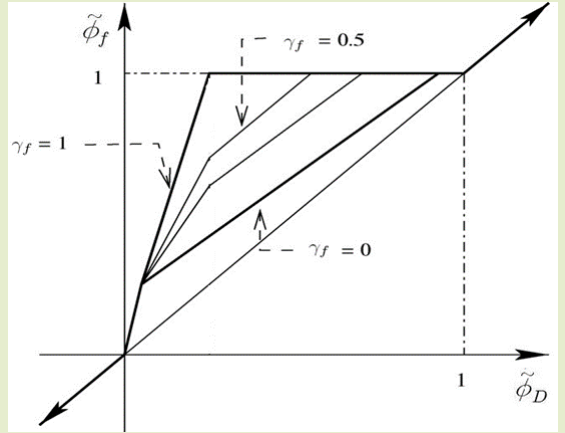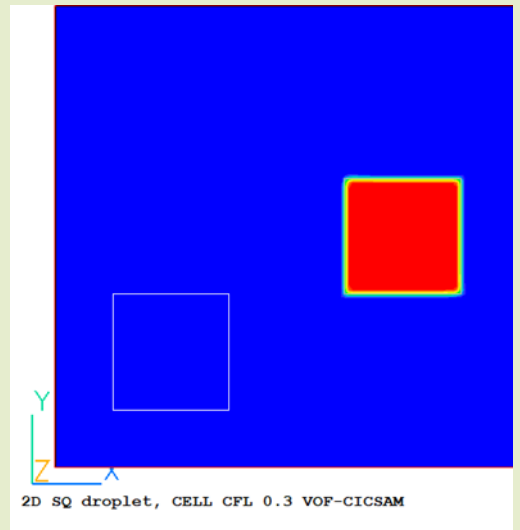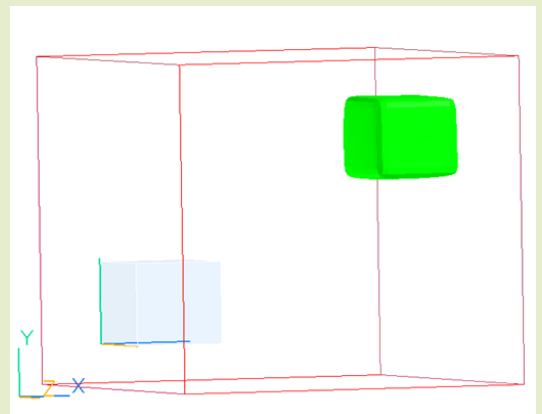*Figure 1: Schematic view of the donor-acceptor scheme.*

Figure 2: NVD for the CICSAM scheme.

Squared water drop in an oblique air flow in 2D after 0.3s. Initial drop at the light square. Using VOF-CICSAM.

Squared water drop in an oblique air flow in 3D after 0.3s. Initial drop at the light square. Using VOF-CICSAM.

CICSAM: Compressive Interface Capturing Scheme for Arbitrary Meshes

The CICSAM scheme [Ubbink 1997] blends the Hyper-C and ULTIMATE-QUICKEST (UQ) schemes, with a blending factor of γ_f based on the angle between the interface and the direction of motion. This scheme can be applied to arbitrary meshes. The Hyper-C scheme is defined as follows

$$\widetilde{\phi}_{fCBC} = \begin{cases} \min\left(1, \dfrac{\widetilde{\phi}_D}{C_f}\right) & for \ \ 0 \le \widetilde{\phi}_D \le 1 \\ \widetilde{\phi}_D & for\,\widetilde{\phi}_D \notin [0,1] \end{cases} \qquad (2)$$

The scheme satisfies the CBC criterion, and is compressive; which may in some situations deform the shape of the interface. The scheme is therefore blended with a less diffusive UQ scheme which has been derived from the QUICK scheme, and is defined as follows:

$$\widetilde{\phi}_{fUQ} = \begin{cases} \min\left(\dfrac{8C_f\widetilde{\phi}_D + (1-C_f)(6\widetilde{\phi}_D + 3)}{8}, \widetilde{\phi}_{fCBC}\right) & for \ \ 0 \le \widetilde{\phi}_D \le 1 \\ \widetilde{\phi}_D & for\,\widetilde{\phi}_D \notin [0,1] \end{cases} \qquad (3)$$

A smooth blend between the Hyper-C and UQ schemes is ensured by the blending factor $0 \le \gamma_f \le 1$ as follows:

$$\widetilde{\phi}_f = \gamma_f \widetilde{\phi}_{fCBC} + (1 - \gamma_f)\widetilde{\phi}_{fUQ} \qquad (4)$$

Where

$$\gamma_f = \min\left(\frac{1 + \cos 2\theta_f}{2}, 1\right) \qquad (5)$$

$$\vartheta_f = \arccos|dn|, \qquad (6)$$

where **n** is the normal vector of the interface, and **d** is the vector parallel to the line between the centers of the donor and acceptor cells. The NVD of the CICSAM scheme is presented in Figure 2.. Similarly, the HRIC, MHRIC and STACS schemes are described in their respective articles.

CSF Model for Surface Tension Force

In this model a volume force due to surface tension on fluid elements lying within a finite-thickness transition region replaces discontinuities instead of a surface tensile force, or boundary condition applied as a discontinuity.

The CSF formulation uses the fact that numerical models of discontinuities in finite-volume and difference schemes are continuous transitions within which fluid properties vary smoothly from one fluid to another. The volume force in the CSF model is calculated by taking first- and second-order spatial derivatives of the characteristics data, which here is the colour-function value. At each point within the free-surface transition region, a cell-centered value is defined proportional to the curvature of the constant colour-function surface at the point. Using the formulation of Brackbill et al (1992), we have:

$$F_{st} = \sigma\kappa\frac{\nabla C}{[C]}\frac{\rho}{\left(\dfrac{\rho_1 + \rho_2}{2}\right)}\delta \qquad (7)$$

where, F_{st} is the surface-tension body force, C is the filtered colour function, σ is the fluid surface-tension coefficient, ρ is the density, ρ_1 and ρ_2 are the densities of phase 1 & 2 respectively, δ is the Kronecker delta function, κ is the free-surface mean curvature defined as:

$$\kappa = \frac{1}{|\vec{n}|}\left[\left(\frac{\vec{n}}{|\vec{n}|}\cdot\nabla\right)|\vec{n}| - (\nabla\cdot\vec{n})\right] \qquad (8)$$
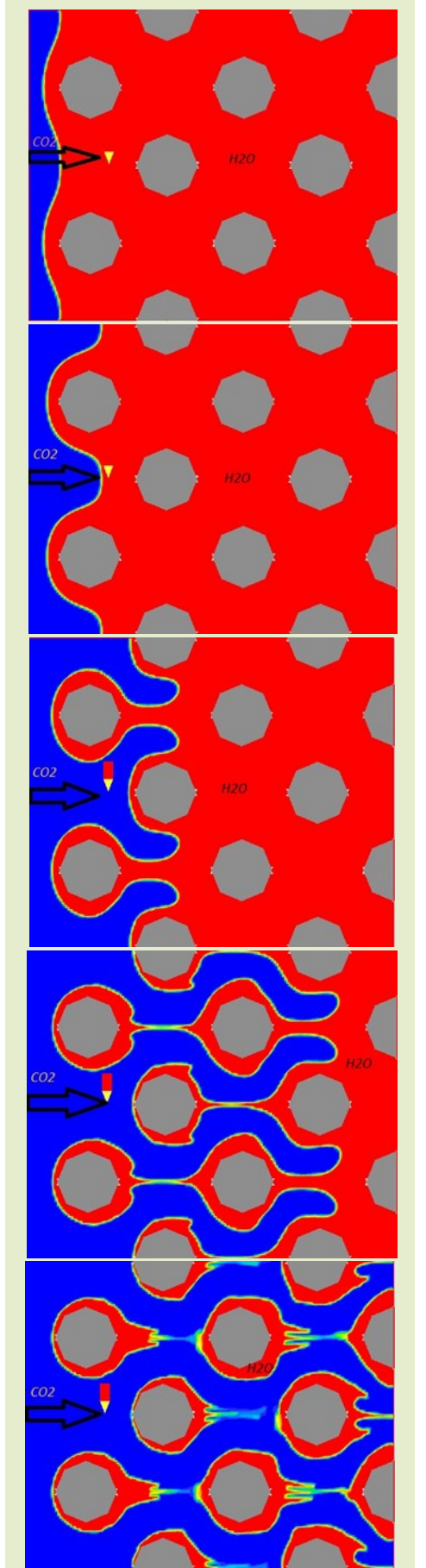
Near Critical CO2 flowing in a channel with octagonal micropillars filled with water. At different instant in dimensionless time: 0.28, 0.52, 1.04, 2.04.

[C] is the difference of the colour function across the interface, and

$$\vec{n} = \nabla C \qquad\qquad (9)$$

Practically, the term F_{st} is a force vector source decomposed into three components along the X, Y & Z directions. Each component provides a momentum source term for the corresponding velocities, similar to the gravitational force, except that it is always for the three components of velocity.

Verification

The methods have been tested in 2D and 3D configurations from circular drop, squared drop, two phases with solid objects. Many of the animations can be seen at www.facebook.com/arcofluid . A few examples obtained using the CICSAM method are shown on sidebars on pages 2 and 3.

MHRIC and STACS have proven superior to other methods when the local CFL number is bigger than 0.45. We have tested these methods using the Zalesak disk in a fixed rotating velocity field. This case is a well-known benchmark for free surface numerical methods; one can observe if the shape of the slotted disk is retained during rotation around the red spot.
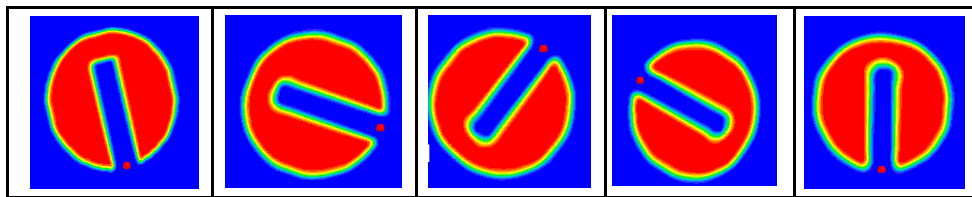

Zalesak disk case: Heavy fluid in red (Water), Light fluid in blue (Air). Number of cell in X&Y direction: 200 x 200. Timestep: 7.95 10^{-4}. Method used here is the STACS algorithm. We have a well preserved shape of the slotted disk. Diameter of the disk 25 cm. Rectangular slot inside the disk: 5cmx20cm.

We have applied the VOF STACS method to a classical Rayleigh Taylor problem in hydrodynamics where we have a heavy fluid (Mercury) on top of a lighter fluid (Paraffin Oil). This setup leads to the well-known Rayleigh-Taylor instability. We can observe, at an early stage, the formation of viscous finger due to the low viscosity of Mercury relative to the Paraffin Oil. In the sequence of figures below we show the colour function at different time steps in a cavity of 4m x 1m. To start the movement, we impose a sinusoidal interface. The surface tension development, is also applicable to the previous two-phase flow methods in PHOENICS: HOL and SEM.

The new VOF techniques enlarge the field of application for PHOENICS and are available via its VR menu. Features allowing the handling of a variable surface tension with temperature (Marangoni flows) and evaporation/condensation effects using the VOF technique will be added in the near future.

| T=0.01s | T=0.3s | T=0.6s | T=0.9s |

T= 1.2s	T=1.3s	T=1.6s	T=2.0s
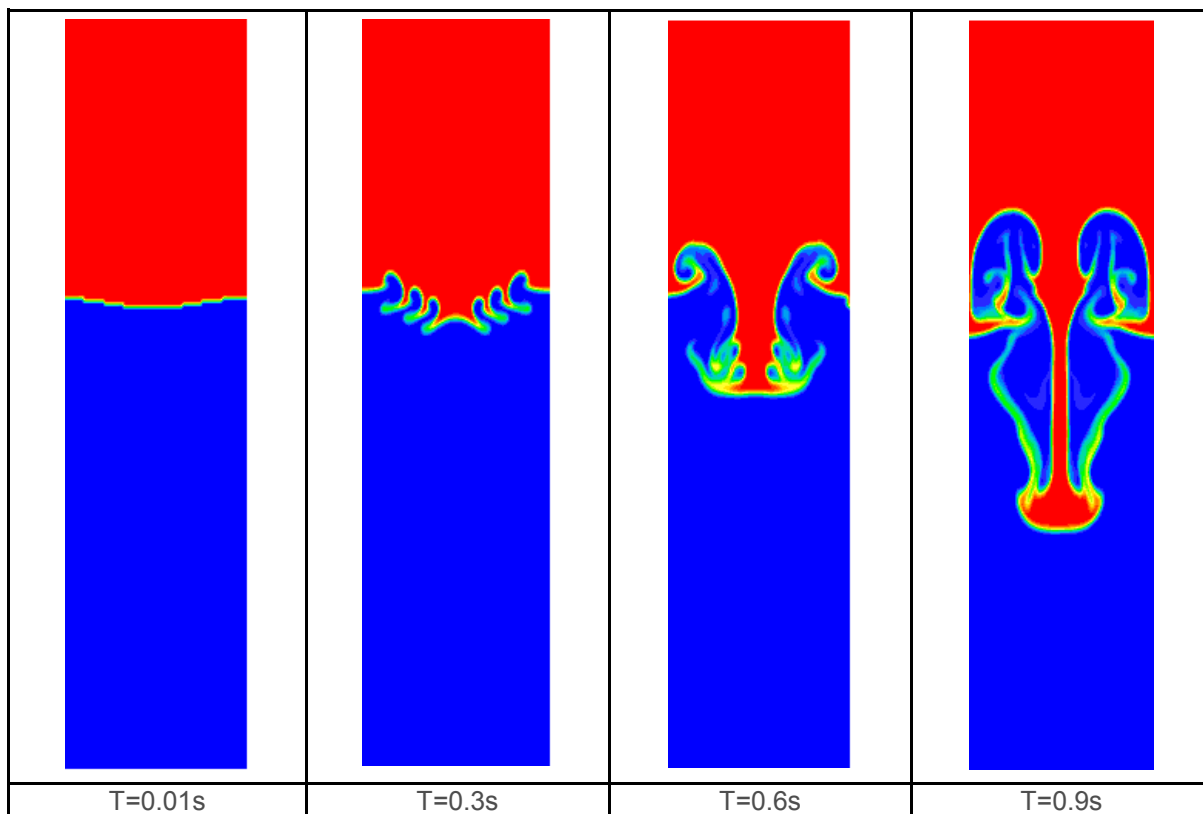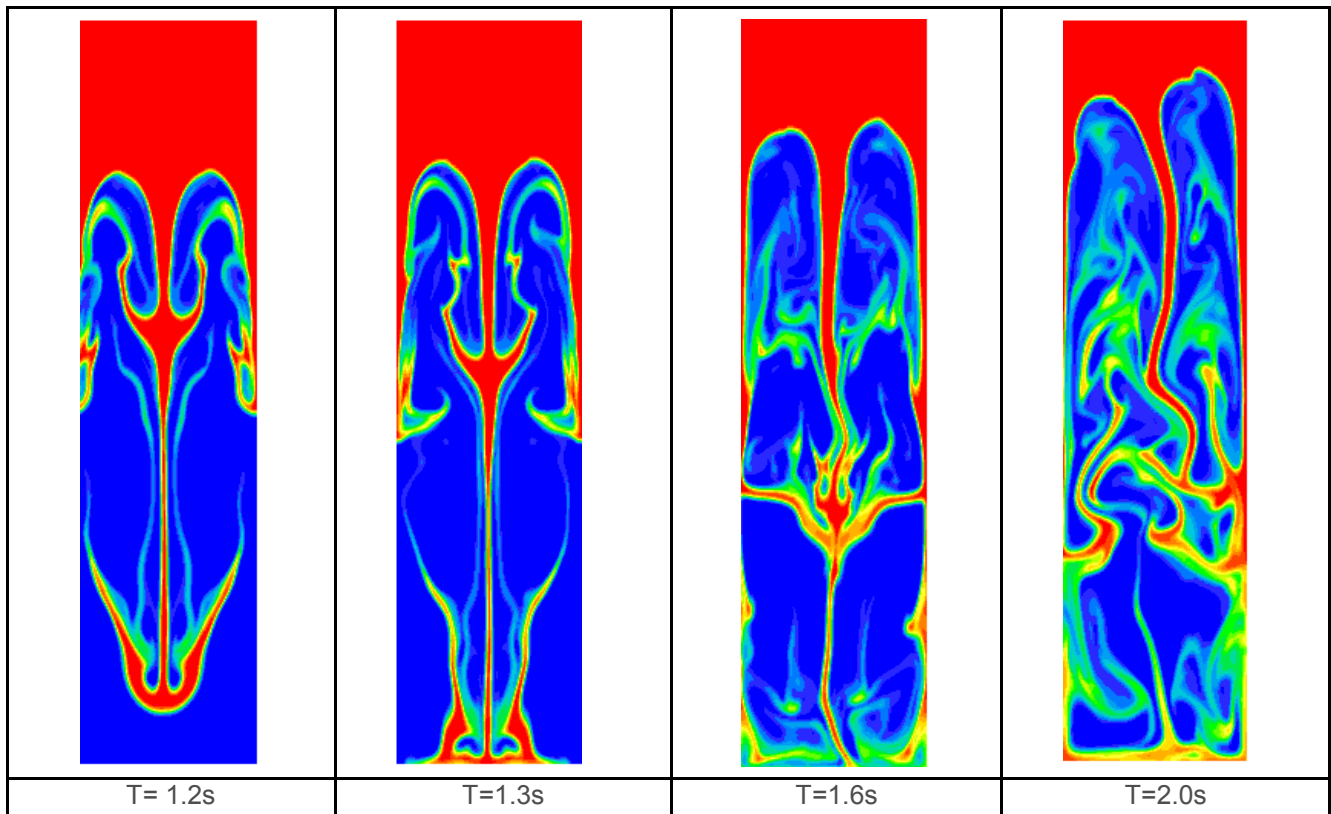
References

1) Ubbink, O. and Issa, R., 1999. A method for capturing sharp fluid interfaces on arbitrary meshes. Journal of Computational Physics 153, 26-50.

2) Ubbink, O., 1997. Numerical prediction of two phase fluid systems with sharp interfaces. Ph.D. thesis, University of London.

3) Muzaferija, S., Peric, M., Sames, P., Schelin, T. A two-fluid Navier-Stokes solver to simulate water entry. 1998 *Proc. Twenty-Second Symposium on Naval Hydrodynamics*

4) Park, I.R., Kim, K.S., Kim, J., and Van, S.H., "A Volume-Of-Fluid Method for Incompressible Free Surface Flows," Int. J. Numer. Meth. Fluids, Vol. 61, pp. 1331-1362, 2009.

5) Darwish, M., Moukalled, F. Convective Schemes for Capturing Interfaces of Free-Surface Flows on Unstructured Grids. *Numerical Heat Transfer Part B*, 2006, Vol. 49, pp. 19–42.

6) Wacławczyk, T., Koronowicz, T. Comparison of CICSAM and HRIC high resolution schemes for interface capturing *Journal of Theoretical and Applied Mechanics*, 2008, Vol. 46, p. 325–345.

7) Leonard, B.P. The ULTIMATE conservative difference scheme applied to unsteady one-dimensional advection. *Comp. Meth. in Appl. Mech. and Eng.*, 1991, Vol. 88, p. 17–74.

8) J.U. Brackbill, D.B. Kothe and C. Zemach, "A continuum method for modeling surface tension", J. of Computational Physics, Vol. 100, p. 335, 1992.

Modelling of Waves Formed from Landslides into the Sea

Dr R. P. Hornby e-mail: bob.hornby007@gmail.com

Introduction

Tsunamis (figure 1) have been thought to be principally caused by earthquakes and so not considered to be a threat to the United Kingdom (UK). However, more recent studies (Ref 1) have shown that large scale underwater landslides can also trigger tsunamis and that such events have happened at least 6 times north of the British coastline over the past 20,000 years – one such event 8,200 years ago generating a 20m high tsunami in Shetland. The risk may appear to be low, but nuclear and other essential service installations are required to be protected against disasters occurring more than once every 10,000 years. In addition the likelihood of landslides in the sea is set to increase with climate change as increased temperatures promote the sudden release of large volumes of ice and silt into the northern seas.

It is important to be able to predict the initial structure of the wave produced by these events. This 'local' information can then be input into models that propagate the disturbance out into the open sea. In order to illustrate the initial wave formation, the PHOENICS Scalar Equation Method (SEM) has been used. For an example of the use of the SEM and comparison with experiment see Ref 2. Here it is used to predict the waves produced in two cases, first by a solid mass plunging into the sea with prescribed velocity and second by the collapse of a warmed bank of glacial debris (treated as a fluid). These can be considered to represent the two extremes of debris collapse into the sea.

Figure 1. Tsunami wave overrunning protective barriers in the Japanese city of Miyako in 2011 (Ref 1)

PHOENICS Modelling

In the first case a 3-D Cartesian domain 100m by 150m by 30m in the *x*, *y* and *z* directions is used with the *x* direction lateral, the *y* (wave) direction axial and the *z* direction vertical. This domain is discretised uniformly in each direction using respectively 50, 150 and 60 cells. The time step is chosen to give a Courant Number less than 1.0. Sea water (density taken as 998.2kg/m³) fills the domain to a depth of 10m with air (density 1.2kg/m³) above.

A constant pressure boundary condition is applied on the upper surface of the domain. All other boundaries are solid and frictionless, with solid lateral boundaries used for computing convenience. Using the PHOENICS MOFOR procedure, a solid cylinder of lateral length 60m and diameter 10m (representing a land mass collapse) plunges into the sea with prescribed *y* and *z* direction velocities (figure 2) that produce an angled trajectory with the debris ultimately at rest on the sea bottom.

The results after 6.7s (when the solid mass is close to the sea bottom) are shown in figure 3. A 4m high wave is formed travelling ahead of the cylinder with a smaller depression (2.5m in magnitude) travelling back towards land.
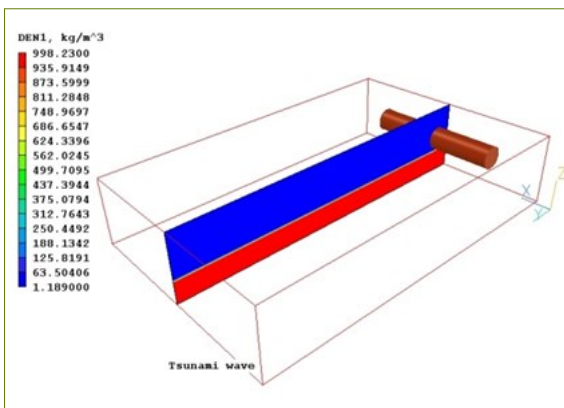

Figure 2:
Left: Initial situation.
Right: Prescribed
y (green) and z (blue)
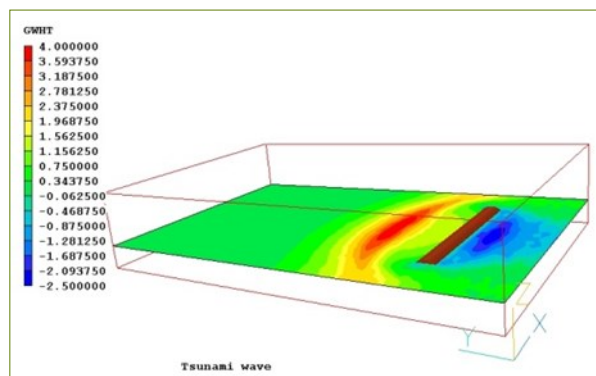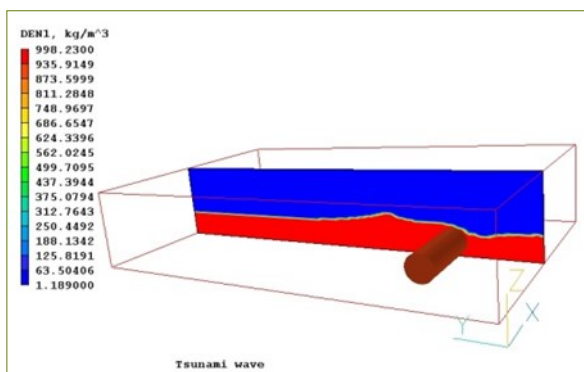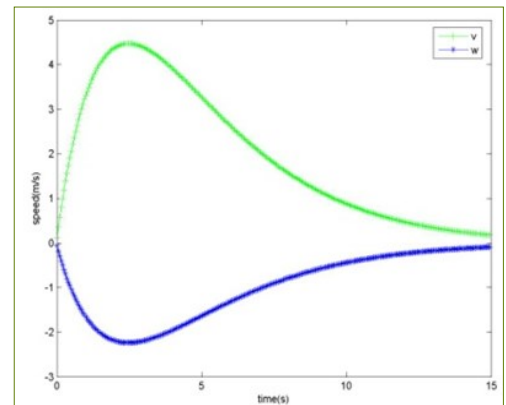*direction cylinder*
speeds.

Figure 3. The wave formed after 6.7s when the collapsed land mass is close to the sea floor. Left, section through the central section of the collapsed land mass showing the distribution of water and air. Right, wave heights as a function of x and y.

In **the second** case, the same domain and discretisation are considered. A cliff of ice debris 60m by 15m by 20m (figure 4) is assumed to be destabilized by warming and to slump as a liquid (with the same density as the seawater) into the adjacent sea.

The wave heights above sea level are shown in figure 5 for 3s and 6s after the cliff collapse. Waves of height 8m and 5.5m are formed, respectively.

Figure 4. Initial situation. 60m x 15m x 20m section of ice debris cliff (in red) destabilized by warming. Sea level as in figure 2.
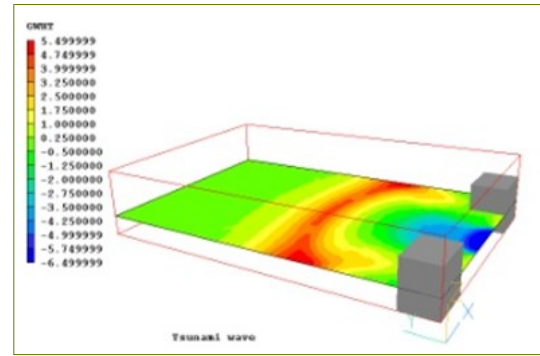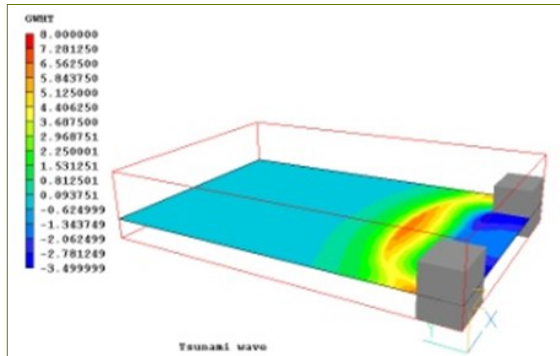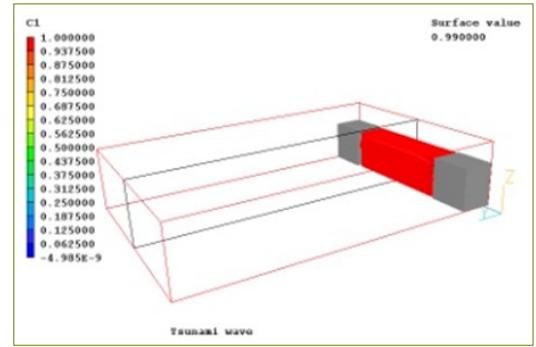

Figure 5. Left, wave heights 3s after cliff collapse. Right, wave heights after 6s.

To explore in more detail a possible relationship between the amount of material slumping into the sea and the wave height produced, a 2-D version of the second case is employed with the y direction extended to 300m. This model would be economically suitable for large stretches of landslide into the sea where there is only a relatively small lateral variation in conditions. Seven cases are considered with varying amounts of slumping debris per unit lateral length of cliff. A typical sea surface profile is shown in figure 6, 18.1732s after the collapse of an ice debris cliff 15m in height above sea level and extending 20m seaward.

For each case the maximum wave height squared after 20s from collapse is plotted against the slumped material potential energy per lateral length (MJ/m) of cliff at time t=0. The results, shown in figure 7, produce a reasonable correlation between the wave height at 20s and the potential energy of the collapsed debris. This is an expected but not a general result as, for example, no wave breaking occurred in the simulations considered.
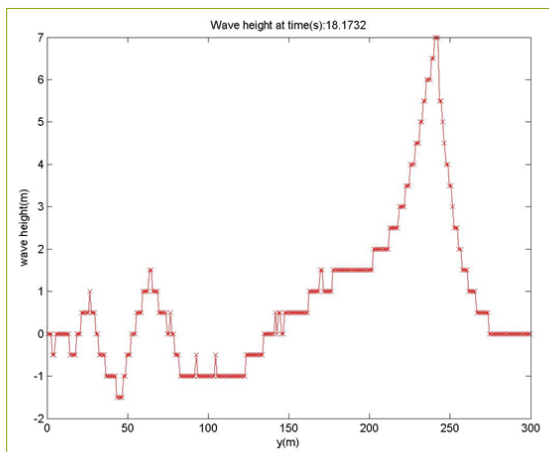

Figure 6. Typical sea surface profile 18.1732s after cliff Ice debris collapse
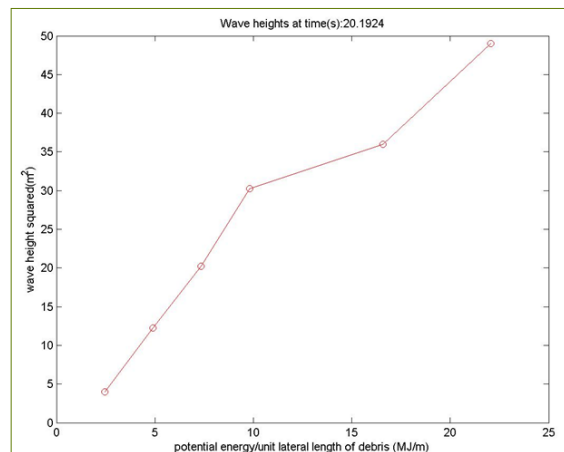

Figure 7. Wave heights squared plotted against potential energy of slumping material

Conclusions

The PHOENICS SEM (in conjunction with MOFOR) has been used to illustrate the initial stages of wave formation from landslides into the sea. These methods can be adapted for specific cases of interest to determine the initial wave structure for input into models propagating the waves out into the far reaches of the sea (e.g. Ref 3).

References

1) J. Leake. Undersea landslides threaten Britain with tsunamis. Sunday Times , 4th December 2016.
2) PHOENICS modelling of 3-D flow over a surf reef and comparison with experiment. PHOENICS Newsletter, Winter 2012.
3) MOST (Method Of Splitting Tsunami) model. NOAA Centre for Tsunami Research. (nctr.pmel.noaa.gov/model.html).

Development of a Sustainable System of Decentralized Mechanical Ventilation for Façades

Marco Aurélio de Oliveira - Director, Civil Engineer - Acoustic Consultant
University of Minho, International Doctoral Programme in Sustainable Built Environment
www.confortus.com, Telemóvel: 963 630 381

Introduction

The product development presented below is the result of a partnership between CHAM and the International Doctoral Programme in Sustainable Built Environment of the University of Minho in Portugal. The simulations using PHOENICS and PHOENICS-Flair were very important to evaluate the thermal and ventilation performance of a prototype that is being developed by PhD student Marco Aurélio de Oliveira. The prototype consists of a sustainable decentralized mechanical ventilation system for use in façades, capable of combining normative acoustic, ventilation and thermal requirements. A geometry was initially created in PHOENICS to assess air velocity and temperature, as shown in Figures 1 and 2 below.
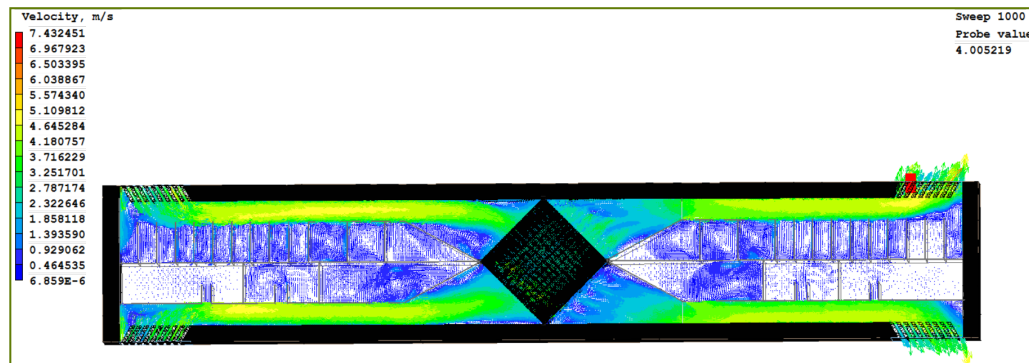

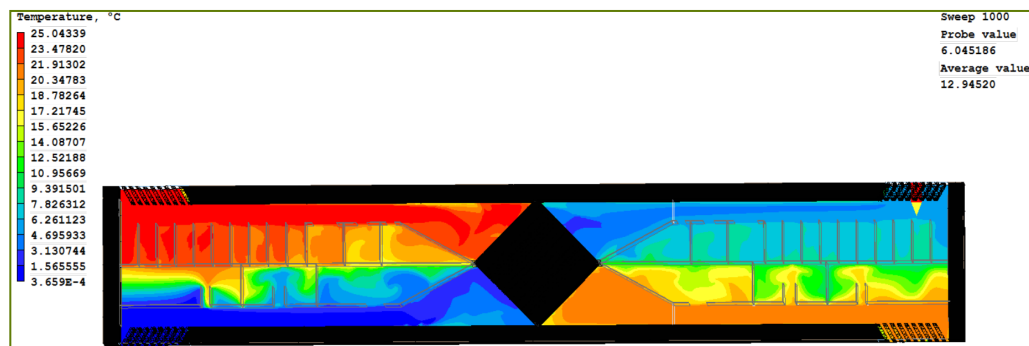*Figure 1: PHOENICS: CFD air speed simulations*

Figure 2: PHOENICS: CFD temperature simulations

In the central part of the prototype there is a heat recovery system and the driven forces, in the two circuits, arise from two small internal motors. The results of such simulations were then used in PHOENICS -Flair to evaluate the air circulation velocity as well as thermal comfort conditions in a virtual study environment. Figures 3 and 4 below show some of the results of these CFD simulations.
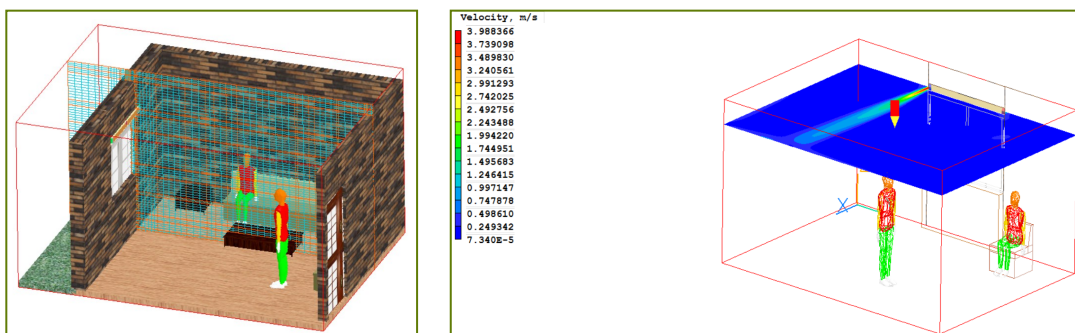

Figure 3: PHOENICS-Flair: geometrical model and simulation of the air circulation velocity.

Results

The results of the simulations showed that the prototype, within the configured parameters tested, met all the ventilation and thermal comfort requirements of Portuguese standard NP 1037-1 and standard CEN 15251-2006.

Conclusions

CFD simulations with PHOENICS permitted adjustment and modification of the shape and materials of the prototype until it resulted in a final design solution, which will be the guideline for the manufacture and subsequent evaluation of a physical prototype in a laboratory. Thus, it was possible to establish an effective and efficient desigh solution during product development whilst avoiding costs associated with the construction and physical testing of preliminary designs.

The use of PHOENICS and PHOENICS -Flair was central to our work as researchers and was a powerful and advanced tool in this regard. We would like to thank CHAM and especially Mr Peter Spalding. Without them, this stage of our research would not have been possible.
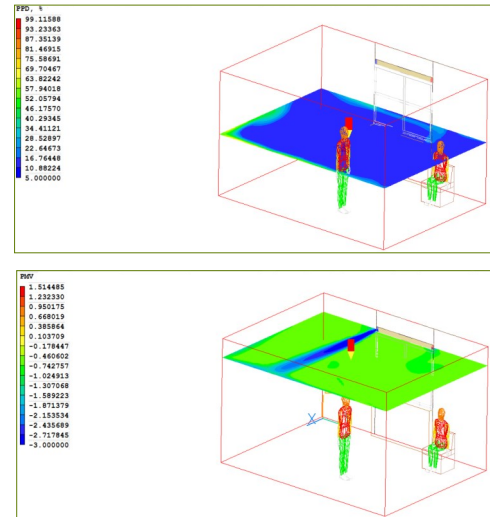
Figure 4: PHOENICS-Flair: thermal comfort simulation

Aerosol Deposition Modelling with PHOENICS-FLAIR 2017 V2

Bin Zhao[1], Bin Zhou[1] and Michael Malin[2]

In an earlier Newsletter article [1], an Eulerian-based multi-phase model was described for simulating the dispersion and deposition of aerosol particles in indoor environments. This model has now been implemented as a standard option in the forthcoming release of PHOENICS-FLAIR 2018. Typical applications include studying indoor air quality and designing ventilation systems to deal with: human exposure to biological or radiological aerosols in healthcare or laboratory environments; health hazards from industrial aerosols; protective environments and isolated clean rooms; and surface contamination of artworks, electronic equipment, etc.

The aerosol model assumes a very dilute particle phase (one-way coupling) with no collisions or coalescence, and drift-flux modelling is used to represent slippage between the particle and gas phases due to gravitational effects [2]. In practice, aerosols can be deposited on surfaces by various mechanisms, including particle inertia, gravitational settling, Brownian diffusion (where particles are transported towards the surface as a result of their collisions with fluid molecules), turbulent diffusion (where particles are transported towards the surface by turbulent flow eddies), turbophoresis (where particles migrate down decreasing turbulence levels as a result of interactions between particle inertia and inhomogeneities in the turbulence field) and thermophoresis (where temperature gradients drive particles towards or away from surfaces).

The PHOENICS model considers all these mechanisms apart from thermophoresis, which is planned for a future release. The surface-deposition fluxes themselves are calculated by using semi-empirical wall models [3-7] as a function of particle size, density and friction velocity, and the deposition rates are reported automatically for all surfaces by the CFD solver.

As a validation of the new aerosol model, a numerical study has been conducted to investigate particle deposition from fully-developed turbulent air streams in vertical ventilation ducts and pipes. In this situation, inertial impaction and gravitational settling are absent, and so it provides a test of deposition influenced by molecular and turbulent processes.

Figure 1 compares PHOENICS results of the dimensionless particle-deposition velocity V_d^+ versus dimensionless particle-relaxation time t^+ onto smooth walls with the measured data. The figure also includes results obtained from the semi-empirical methods of Lai and Nazaroff [5] and Zhao & Wu [6].

The dimensionless parameters are defined by: $V_d^+ = V_d/V_*$ and $t^+ = tV_*^2/\nu$ with $t = \rho_p d^2 C/18\rho\nu$, where V^* is the wall friction velocity, C is the Cunningham slip-correction coefficient (which accounts for non-continuum effects on the drag of small particles), d the particle diameter, ρ the density and ν the kinematic viscosity. The particle deposition velocity itself is defined by $v_d = m''/\rho Y$ where m" is the particle-deposition mass flux and Y is the particle mass fraction. The measurements come from several different experiments, and include those of Liu and Agrawal [8] which are widely used to validate particle-deposition models.

From Figure 1, first it can be seen that although the measured deposition rates vary with particle sizes in a similar trend to produce a "S-shaped" curve, there is considerable scatter between the different experiments. This indicates that factors other than particle size also influence the particle deposition rates, such as for example turbulence levels and surface properties. The measurements fall into three distinct categories [9]: (1) At first, as t^+ increases, the deposition velocity decreases. This is the so-called turbulent-diffusion regime (t+<0.1). (2) In the next zone (0.1<t+<10), the so-called eddy diffusion-impaction regime, the deposition velocity increases by three to four orders of magnitude. (3) The third regime of deposition (t+>10), usually termed the particle-inertia-moderated regime, results in an eventual decrease in V_d for large particle sizes. This ''S-shaped'' curve is regarded as the benchmark for particle deposition from fully developed turbulent flow onto surfaces.

The PHOENICS results agree well with the measured data, and the "S-shaped" curve of deposition velocity versus particle relaxation time is well simulated by the model. Brownian and turbulent diffusion dominate in region (1), where turbophoresis is negligible for small particles.

Turbophoresis, however, is the primary mechanism operating in regions (2) and (3). In region (2) particles have less tendency to follow turbulent air fluctuations, and so there will be interaction between particle inertia and turbulent eddies. In region (3) particles are too large to respond to the rapid fluctuations, and so transport by turbulent diffusion towards the surface is very weak. The failure of the Lai-Nazaroff model in region (3) is because their model doesn't account for turbophoresis.
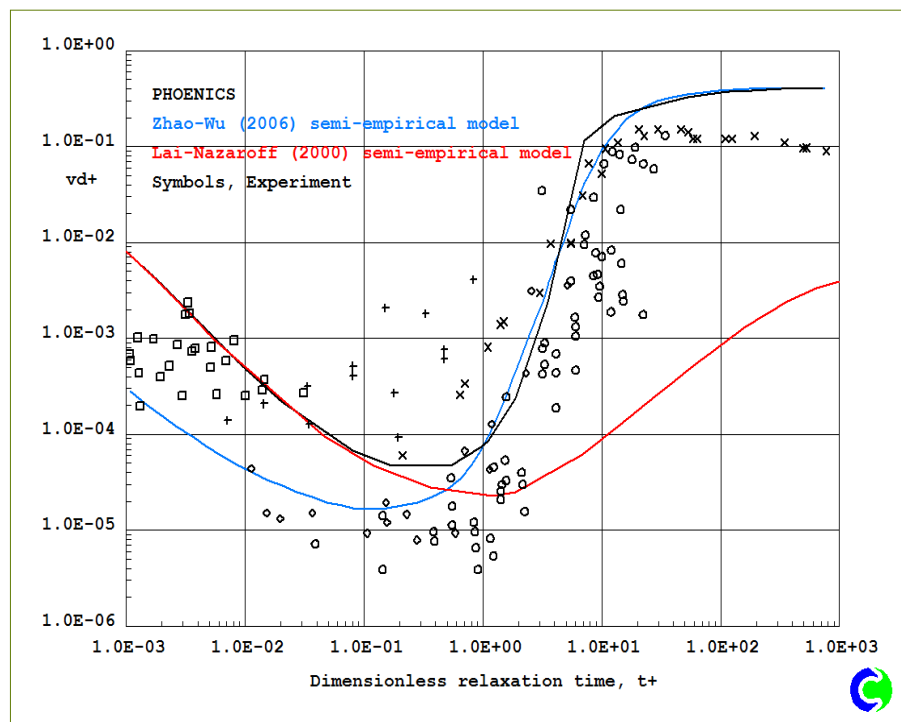

Figure 1: Comparison of measured and predicted particle-deposition rates on smooth vertical duct walls.

References

1) B.Zhao, B.Zhou & M.R.Malin, "PHOENICS Modelling of Indoor Aerosol Transport and Deposition", PHOENICS Newsletter Winter 2015/2016,CHAM Limited, Wimbledon, London, UK, (2016).
2) B.Zhao, C.Chen & Z.Tan, "Modelling of ultrafine particle dispersion in indoor environments with an improved drift flux model", J. Aerosol Science, 40(1), p29-43, (2009).
3) B.Zhao & B.Zhao, "Test of a generalised drift-flux model for simulating indoor particle dispersion", Proc. 7th Int. Symp. on Heating, Ventilation & Air Conditioning, Vol. II, Topic 2: Indoor Environment, 382, (2011)
4) B.Zhao, X.Li & Z.Zhang, "Numerical study of particle deposition in two differently ventilated rooms", Indoor & Built Environment, Vol.13, p443-451, (2004).
5) A.C.K.Lai & Nazaroff, "Modelling indoor particle deposition from turbulent flow onto smooth surfaces", Aerosol Sci. Technol. 31: 463–476, (2000).
6) B.Zhao & J.Wu, "Modelling particle deposition from fully developed duct flow", J. Atmospheric Environment, Vol.40, p457-466, (2006).
7) V.N.Piskunov, "Parameterisation of aerosol dry deposition velocities onto smooth & rough surfaces", Aerosol Science 40 (2009) 664-679, (2009).
8) B.Y.H.Liu & J.K.Agrawal, "Experimental observation of aerosol deposition in turbulent flow", Aerosol Science, Vol.5, p145-155, (1974).
9) A.Guha, "Transport and deposition of particles in turbulent and laminar flow", Ann. Review Fluid Mech., Vol.40, p311-341, (2008).

1 Department of Building Science, School of Architecture, Tsinghua University, Beijing 100084, China.
2 Concentration Heat and Momentum Limited, Wimbledon Village. London SW19 5AU, England.

Implementation of Numerical Wave Generation in PHOENICS Marine

Timothy Brauner, CHAM London

Surface waves are a phenomenon that appears on the interface between two different media (as opposed to body waves travelling through a medium). Of particular interest to engineering applications are the surface waves that occur on the interface of air and water.

Fluid structure interactions, where the structure might be a ship, oil platform, dam or wave breaking structure protecting a port, are of great interest to a number different industries. Designing a ship's hull to meet specific speed and fuel requirements and then analysing its stability in and response to waves by computing the loading and stresses exerted on it, is a prime example of a requirement for wave simulation and the main reason for its implementation in PHOENICS.

Wave height, wave period and water depth are the three major characteristics used to classify waves. Assuming that the water depth is significantly larger than the bottom boundary layer, the flow region under a water wave train is governed by potential flow theory (i.e. viscous effects are negligible and the flow remains irrotational). Numerical modelling of water waves can then be achieved by finding solutions to the potential flow problem. Different levels of approximation of the solution can be used to represent different types of waves.

Fundamentally a water wave can be represented as a sinusoidal function with a set wave height and wave period. This is known as Airy wave theory or 1st order wave theory and is applicable to long and shallow waves. For higher wave heights and shorter wave periods, higher order wave theories are needed, which represent the wave as the sum of multiple interconnected sinusoidal functions.

There are several approaches to modelling higher order waves, the most frequently used is Stokes Wave Theory. Generally the highest order theory used is the 5th order approximation, capable of generating waves up to the limit at which waves would start to break. For very shallow water waves Boussinesq Wave Theory can be used to generate so called cnoidal and solitary waves.

These theories have been implemented into PHOENICS, and RhinoCFD Marine in particular (1st, 2nd and 5th order Stokes waves). These waves are generated at a vertical inflow plane by specifying a time dependent water height and variable mass flow and varying velocity components for the mass and momentum conservation equations respectively. Depending on the user specified wave height, wave period and water depth an appropriate wave theory is selected automatically.

Figure 1 – Below: 5 sine functions (top) of different amplitude and wave length and their sums (bottom) representing 1st, 2nd, 3rd and 5th order waves, Right: wave regime diagram for classification of waves and determination of appropriate model order.
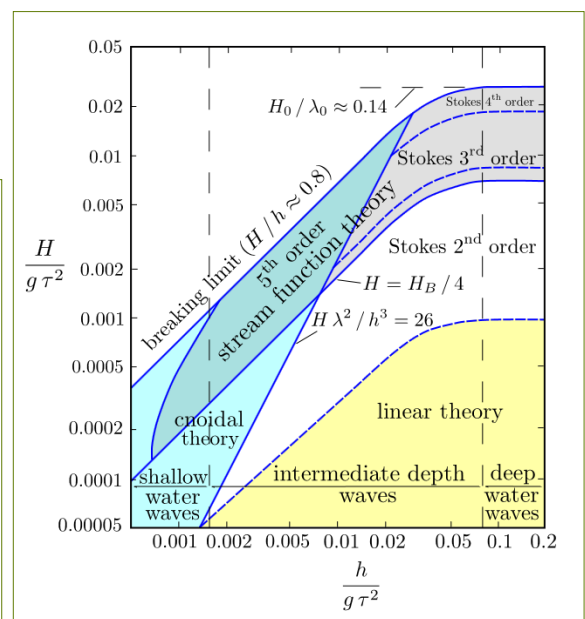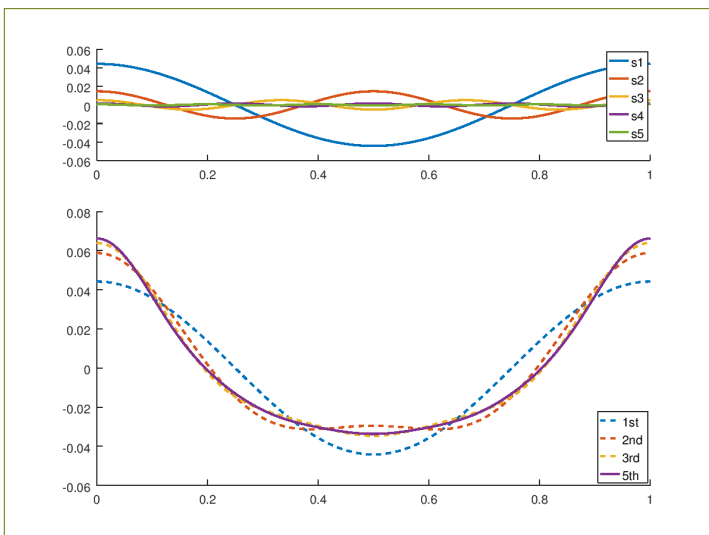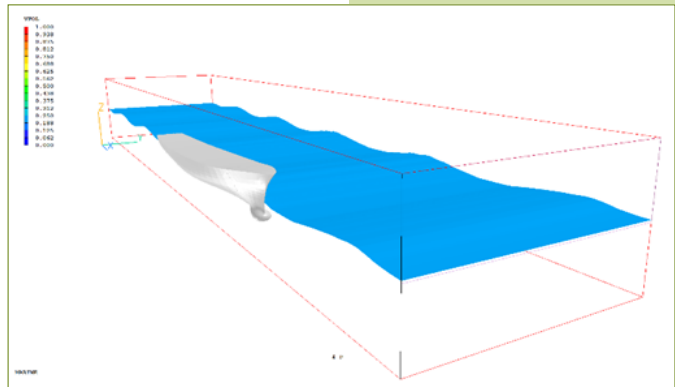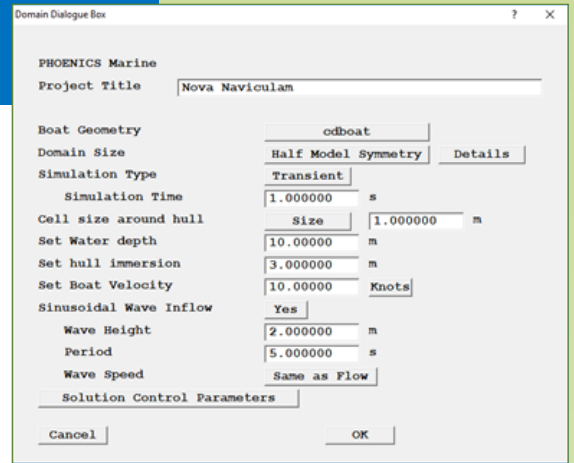
A NEW Product from CHAM

PHOENICS Marine

CHAM is pleased to announce the development and imminent release of its Marine Special Purpose Product which will enable Naval Architects and Marine Engineers to analyse hull performance quickly and effectively, while minimizing the learning curve that CFD usually entails.

Using free-surface methods PHOENICS Marine will allow users to specify a hull shape, and some key parameters of their simulation such as flow velocity and waterline, while fully automating aspects such as domain generation, mesh setup and relaxation parameters. This is done via a brand-new simplified menu interface, wholly dedicated to this type of simulation. The code will return values for drag, separated into skin friction and form drag while displaying and quantifying the size of bow and stern waves produced. An added innovation allows users to test their designs with sinusoidal waves as an input (see pg 11 for full description), and extract parameters such as pressure on the hull as a function of time.

PHOENICS Marine will benefit from current development which will allow for the boat to react dynamically to flow, enabling trim calculations, which are of great interest to naval designers. The Marine SPP will be available for Rhino, where it will be known as RhinoCFD Marine, and should benefit greatly the large number of naval engineers who already use this CAD software.

News from CHAM-Japan

On October 20 2017 CHAM Japan held a PHOENICS User Day at 3-27 Kioi-cho, chiyodaku Tokyo 102-0094. Dr Jeremy Wu represented CHAM and presented PHOENICS-2018. For further information see http://www.phoenics.co.jp/.

CHAM Japan attended DMS Tokyo June 20—23. The PHOENICS Booth was visited by over 100 attendees. http://www.dms-tokyo.jp/en/Home/.

CHAM Japan attended DMS Osaka, http://www.dms-kansai.jp/en/Home/

PHOENICS Booth at DMS Osaka, October 4—6 2017.

Contact Us

We are always pleased to be asked for information about our services and products. call +44 (20) 8947 7651, email sales@cham.co.uk or check for current news on www.cham.co.uk

Staff News

We welcome Louis Rocher who has joined CHAM as an Intern for a 4 month period.

Vacancy

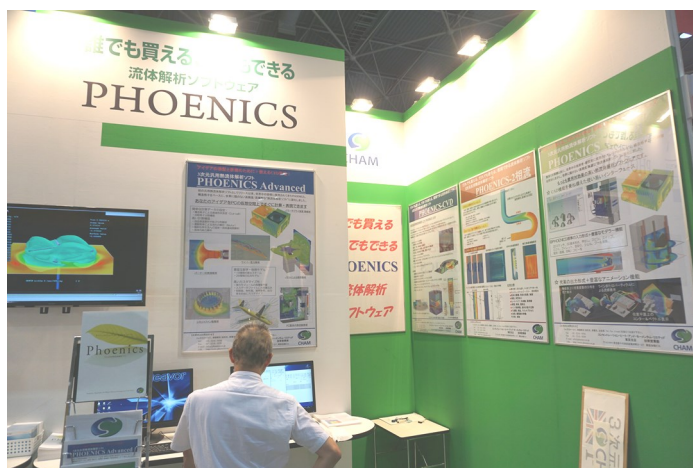**We seek a Junior CAD Engineer with knowledge and expertise in Rhino, C++ and C#, and an interest in developing plug-ins.**

Visit www.cham.co.uk for more information or send your CV to hr@cham.co.uk if you have relevant CAD software qualifications and experience.